Electronic structures and magnetic moments of Co3FeN thin films grown by molecular beam epitaxy

Keita Ito, Tatsunori Sanai, Siyuan Zhu, Yoko Yasutomi, Kaoru Toko, Syuta Honda, Shigenori Ueda, Yukiharu Takeda, Yuji Saitoh, Yoji Imai, Akio Kimura, and Takashi Suemasu

Electronic structures and magnetic moments of Co₃FeN thin films grown by molecular beam epitaxy

Keita Ito,[1] Tatsunori Sanai,[1] Siyuan Zhu,[2] Yoko Yasutomi,[1] Kaoru Toko,[1] Syuta Honda,[1] Shigenori Ueda,[3] Yukiharu Takeda,[4] Yuji Saitoh,[4] Yoji Imai,[1,5] Akio Kimura,[2] and Takashi Suemasu[1,a]

[1]*Institute of Applied Physics, Graduate School of Pure and Applied Sciences, University of Tsukuba, 1-1-1 Tennodai, Tsukuba, Ibaraki 305-8573, Japan*
[2]*Graduate School of Science, Hiroshima University, 1-3-1 Kagamiyama, Higashi-Hiroshima, Hiroshima 739-8526, Japan*
[3]*Synchrotron X-ray Station at SPring-8, National Institute for Materials Science (NIMS), 1-1-1 Kouto, Sayo-cho, Hyogo 679-5148, Japan*
[4]*Condensed Matter Science Division, Japan Atomic Energy Agency (JAEA), 1-1-1 Kouto, Sayo-cho, Hyogo 679-5148, Japan*
[5]*National Institute of Advanced Industrial Science and Technology (AIST), Tsukuba Central 5, 1-1-1 Higashi, Tsukuba, Ibaraki 305-8565, Japan*

We evaluated electronic structures and magnetic moments in Co₃FeN epitaxial films on SrTiO₃(001). The experimentally obtained hard x-ray photoemission spectra of the Co₃FeN film have a good agreement with those calculated. Site averaged spin magnetic moments deduced by x-ray magnetic circular dichroism were 1.52 μ_B per Co atom and 2.08 μ_B per Fe atom at 100 K. They are close to those of Co₄N and Fe₄N, respectively, implying that the Co and Fe atoms randomly occupy the corner and face-centered sites in the Co₃FeN unit cell. © 2013 AIP Publishing LLC. [http://dx.doi.org/10.1063/1.4836655]

3d transition metal ferromagnetic nitrides, composed of abundant elements, have received significant attention for applications in magnetic recording media and spintronics devices. The spin-polarization of electrical conductivity in Fe₄N was calculated to be −1.0, and the spin-polarization of density of states (P) at the Fermi level (E_F) to be −0.60.[1] Larger |P| of 0.88 ($P < 0$) was also theoretically predicted in Co₄N.[2] However, it is difficult to form stoichiometric Co₄N films because the body-centered N atoms tend to be deficient. In our previous work, the diffraction intensity of Co₄N(001) was very weak in the x-ray diffraction (XRD) measurements on Co₄N films.[3] According to the x-ray extinction rule, the diffraction peak of Co₄N(001) is absent when the body-centered N atoms are absent. Thus, we have paid more attention to ternary alloys Co$_x$Fe$_{4-x}$N. Among Co$_x$Fe$_{4-x}$N, first-principles calculation showed that Co₃FeN has larger |P| of 0.75 ($P < 0$) than Fe₄N when Fe atoms are located at the corner (I) sites, and Co atoms at the face-centered (II) sites in the anti-perovskite unit cell as shown in Fig. 1.[4] Epitaxial growth of Co$_x$Fe$_{4-x}$N films has been achieved on SrTiO₃ (STO)(001) substrates by molecular beam epitaxy (MBE)[5] and on TiN/Si(001) using magnetron reactive sputtering.[6] The diffraction peak of Co₃FeN(001) was observed in the XRD patterns,[5] which means that a nitrogen atom is located at the body center of the unit cell of Co₃FeN. However, there have been no experimental reports on the electronic structure and magnetic moments of Co and Fe atoms in these Co₃FeN layers. Theoretical studies about what happens when the Co and Fe atoms are located differently from the above-mentioned ideal case have yet to be investigated. In this study, we aim to

measure the magnetic moments of Co and Fe atoms, and valence band (VB) structures in Co₃FeN films, and compare them with those expected theoretically in order to discuss the Fe and Co sites in the Co₃FeN. We calculated the spin-polarized partial density of states (DOSs) of Co₃FeN. Here, we set Co atoms at sites I and II, and Fe atoms at site II, and used the CASTEP[7] code based on the density-functional theory (DFT) in describing the electron-electron interaction, a pseudopotential description of the electron-core interaction, and a plane-wave expansion of the wave function. As for the method of approximation to the exchange-correlation term of the DFT, we used a spin-polarized Perdew-Wang Generalized Gradient Approximations (GGA-PW).[8] The DOS curves were obtained by broadening discrete energy levels using the Gaussian smearing function of 0.07 eV full-width at half-maximum on a grid of k-points generated by the Monkhorst–Packe scheme.[9] The pseudopotential used is the ultrasoft pseudopotential generated by the scheme of Vanderbilt.[10] Kinetic cutoff energy for expansion of wavefunctions and spacing of sampled k-points in the reciprocal space were set to be 400 eV and 0.5 nm^{-1}, respectively, which correspond to 24 × 24 × 24 Fast-Fourier Transformation arid 7 × 7 × 7 mesh parameters (the number of the sampled k-points from the irreducible part of the Brillouin zone are 172), respectively. These values have been confirmed to be sufficient to obtain well-converged results. We also calculated the value of the magnetic moments for each atom in the ordered Co₃FeN by using the Bader analysis[11] and the VASP package[12] with the projected-augment wave pseudopotential[13] and a spin-polarized GGA-PW method.[8] The optimized lattice structure, a cutoff value of the plane waves of 400 eV and the k-points sampling of 11 × 11 × 11 are used for the calculation of the charge density with VASP package. In our
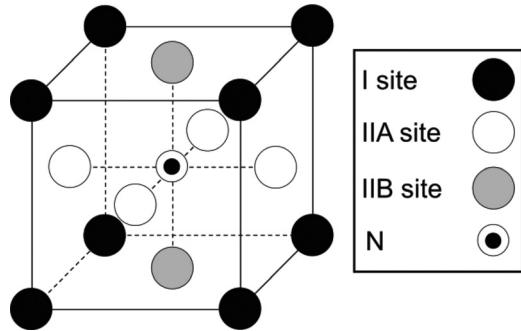
FIG. 1. Lattice structure of anti-perovskite type ferromagnetic nitrides. II sites are distinguished by IIA and IIB sites due to the orientation of the internal magnetic field.
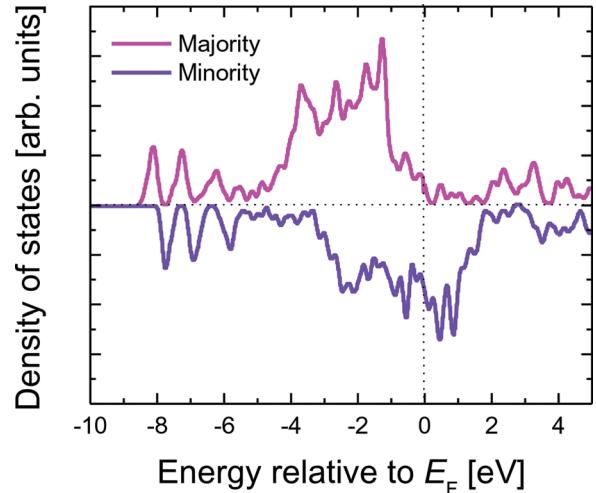

FIG. 2. Calculated total DOSs of majority and minority spins in Co_3FeN, which assumed Co atoms are located at both I and II sites, and Fe atoms located at II sites of the anti-perovskite structure.

framework of first-principle calculations, we cannot take into account thermal effects at the finite temperature to the DFT calculation.

Hard x-ray photoemission spectroscopy (HAXPES) and x-ray magnetic circular dichroism (XMCD) measurements were performed in the $CaF_2(2\,nm)/Co_3FeN(10\,nm)$ layered structure grown on the STO(001) substrate using MBE. Details of epitaxial growth procedures of Co_3FeN films are shown in Ref. 5. HAXPES measurements were performed at the undulator beamline BL15XU[14] of SPring-8 in Japan. We measured VB structures of the Co_3FeN film at 300 K using incident light with a photon energy of 5953 eV and overall energy resolution of 230 meV. The angle of incident light was 88° relative to the surface normal. The CaF_2 capping layer has a large band gap energy (12.1 eV),[15] and therefore the VB of CaF_2 is located far below that of Co_3FeN. This means that the contribution of the CaF_2 layer to the measured VB spectrum can be neglected.[16] Obtained VB spectrum was compared with the photoemission spectrum deduced from the results of the above mentioned first-principles calculation. XMCD measurements were performed at the undulator beamline BL23SU[17] of SPring-8. We measured x-ray absorption spectra (XAS) and XMCD spectra at Co and Fe $L_{2,3}$-edges using the total electron yield method and deduced orbital (m_{orb}) and spin (m_{spin}) magnetic moments per Co and Fe atoms in the Co_3FeN film. Circularly polarized x-rays were incident perpendicular to the sample surface at 100 and 300 K. External magnetic fields of $\pm3\,T$ were applied to Co_3FeN[001] direction (perpendicular to the sample surface) during measurements, and we used their averaged spectra for analysis of magnetic moments to ensure the accuracy of the measurement. 3 T was enough to saturate the magnetization of the sample. On the basis of the obtained magnetic moments, we estimated positions of Co and Fe atoms in the Co_3FeN unit cell.

Figure 2 indicates the calculated spin-polarized partial DOSs of the modeled Co_3FeN. We deduced P to be -0.63 at E_F, which means that $|P|$ is decreased when the Co and Fe atoms are located differently from the ideal case shown in Ref. 4.

Figure 3(a) shows the VB spectrum of the Co_3FeN film measured by HAXPES, and Fig. 3(b) exhibits the calculated photoemission spectra of Co $3d$, $4s$, and Fe $3d$, $4s$ states and their summation in Co_3FeN. These calculated spectra were deduced from the calculated partial DOSs of Co_3FeN

multiplied by the photo-ionization cross-sections at a photon energy of 6 keV.[18] We did not take the N $2s$ and $2p$ states into account because those photoemission intensities were negligibly small, and we were not able to calculate the Co and Fe $4p$ states because there have been no reports so far on the photo-ionization cross-sections of these states.[16] Structures labeled A-D in Fig. 3(a) correspond to those labeled a-d in Fig. 3(b). Structures A-C mainly consist of the Co $3d$ state, and structure D is explained by the Co $4s$ state. The obtained VB spectrum was well fitted to the simulated
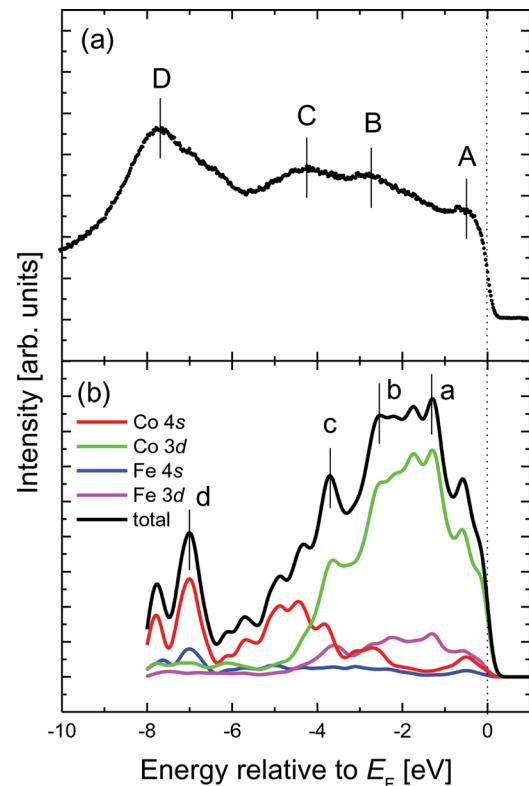

FIG. 3. (a) HAXPES spectrum for Co_3FeN at a photon energy of 5953 eV. (b) Calculated photoelectron spectra for Fe $3d$ and Fe $4s$ electrons in Co_3FeN.

spectrum using the first-principles calculation. However, it is difficult to discuss the sites of Co and Fe atoms in the Co_3FeN film just by comparing the observed VB spectra with those calculated. As reported in Ref. [19], the difference in the whole shape of VB structures between ordered and disordered metal alloys is very small.[19]

Figures 4(a) and 4(b) display the XAS and XMCD spectra at Co $L_{2,3}$-edges in the Co_3FeN film at 300 K, respectively. Distinct MCD signal was observed at Co $L_{2,3}$-edges. In Fig. 4(a), we can see the satellite peaks by approximately 2−3 eV higher than the main peaks of $L_{2,3}$-edges, which are also observed in the reported XAS spectra of Fe_4N and Co_4N films.[20–22] We considered that these satellite peaks were attributed to atoms located at the face-centered sites. Details of this examination will be reported elsewhere. Figures 5(a) and 5(b) present the XAS and XMCD spectra at Fe $L_{2,3}$-edges in the Co_3FeN film at 300 K, respectively. The structure of F K-edge is attributed to the CaF_2 capping layer. Distinct MCD signal was observed at Fe $L_{2,3}$-edges, which have the same sign as those of Co $L_{2,3}$-edges. This means that ferromagnetic order is created between Co and Fe atoms. We also note here that there are small satellite peaks by approximately 2−3 eV higher than the main peaks of Fe $L_{2,3}$-edges. The site-averaged m_{orb} and m_{spin} per Co and Fe atoms of the sample were deduced by applying magneto-optical sum-rules analysis.[23–25] The backgrounds of the XAS spectra were removed by subtracting the two step function from the raw XAS spectra. The electron hole numbers of $3d$ orbital (N_h) of Co and Fe in the sample were determined to be 2.43 ± 0.23 and 4.31 ± 0.70, respectively, from the XAS spectra of the sample by referring to the standard XAS spectra of hcp-Co and bcc-Fe, and N_h values in
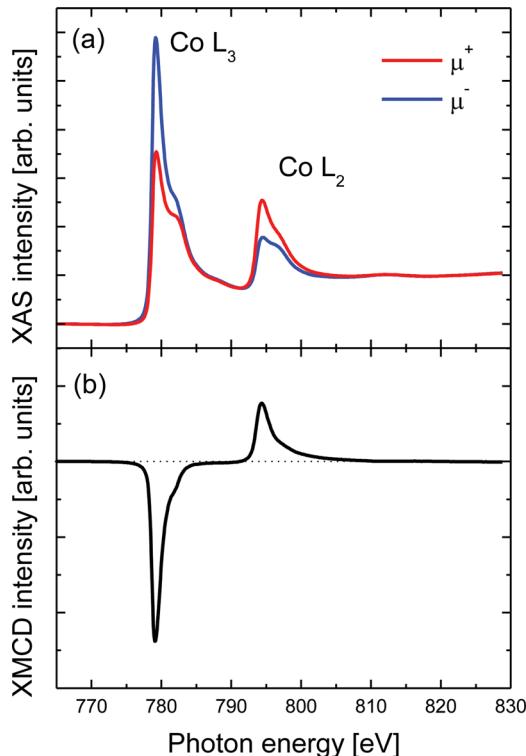

FIG. 5. XAS and XMCD spectra of Fe $L_{2,3}$ edges of Co_3FeN observed at 300 K. The external magnetic field of ± 3 T was applied perpendicular to the sample surface.
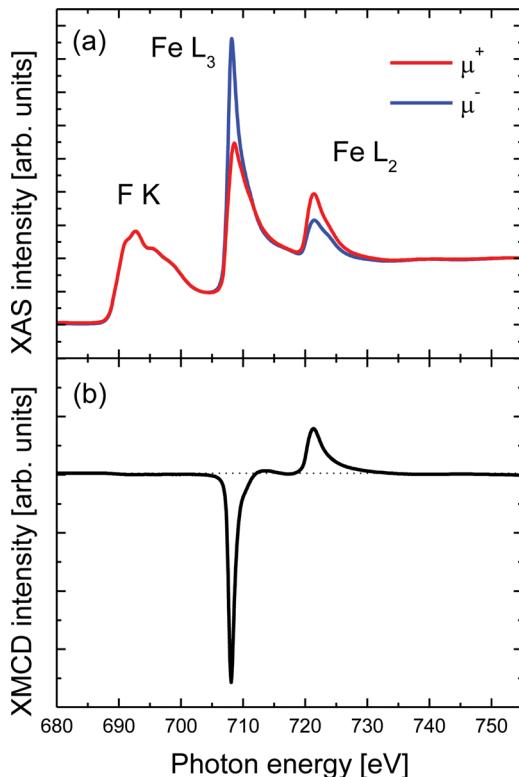
hcp-Co (2.49) and bcc-Fe (3.39).[20,25] The site-averaged m_{orb}, m_{spin}, and sum of them (m_{total}) of the sample are summarized in Table I. The reported values of the magnetic moments of Co_4N and Fe_4N are also shown for comparison.[20,22,26,27] The m_{total} value per Co atom was evaluated to be $1.44 \pm 0.13 \mu_B$ at 300 K and $1.51 \pm 0.17 \mu_B$ at 100 K. For Fe atom, it was deduced to be $1.84 \pm 0.20 \mu_B$ at 300 K and $1.96 \pm 0.16 \mu_B$ at 100 K. In Table I, magnetic moments corrected by taking the saturation effect[28] are listed in parentheses. We used the correction factors in case that the light is incident normal to the film plane with the 10-nm-thick Co and Fe films, shown in Ref. [28]. We estimated the saturation magnetization of the sample to be 1210 emu/cc at 300 K, using deduced m_{total}. This value is a little smaller than 1310 emu/cc obtained by a superconducting quantum interface device magnetometer at 300 K. We think that the deduced magnetic moments from the XMCD measurement are underestimated. The m_{spin} values are calculated to be 1.97 and 1.49 μ_B, respectively, for Co atoms in Co_4N at I and II sites,[26] and the m_{spin} values to be 3.07 and 2.03 μ_B, respectively, for Fe atoms in Fe_4N at I and II sites.[27] The m_{spin} values for Co and Fe atoms in $CoFe_3N$ are calculated to be 1.76 and 2.32 μ_B, respectively, in case that Co atoms are located at I sites, and Fe atoms at II sites.[29] This means that m_{spin} values are enhanced at I sites, but are decreased at II sites, due to the band hybridization between $3d$ orbit of II site atoms and $2p$ orbit of nitrogen atoms.[29] We calculated the m_{spin} values for Co and Fe atoms to be 1.41 and 3.09 μ_B, respectively, in the ordered Co_3FeN. However, the deduced site-averaged m_{spin} values of Co and Fe atoms in the Co_3FeN film from the XMCD measurements are close to those in Co_4N and Fe_4N, respectively. This

FIG. 4. XAS and XMCD spectra of Co $L_{2,3}$ edges of Co_3FeN observed at 300 K. The external magnetic field of ± 3 T was applied perpendicular to the sample surface.

TABLE I. Orbital, spin, and total magnetic moments of Co and Fe atoms in $Co_xFe_{4-x}N$ deduced by XMCD and theoretical calculations. Corrected moment values of samples after taking the saturation effect into account are listed in parentheses.

Compounds	Atom	Magnetic moment [μ_B per atom]			Method	Reference
		m_{orb}	m_{spin}	m_{total}		
Co_3FeN	Co(300 K)	0.11 ± 0.01	1.33 ± 0.12	1.44 ± 0.13	XMCD	…
	(corrected)	($\sim$0.15)	($\sim$1.47)	($\sim$1.62)		
	Fe(300 K)	0.08 ± 0.01	1.76 ± 0.19	1.84 ± 0.20	XMCD	…
	(corrected)	($\sim$0.16)	($\sim$1.91)	($\sim$2.07)		
Co_3FeN	Co(100 K)	0.13 ± 0.02	1.38 ± 0.15	1.51 ± 0.17	XMCD	…
	(corrected)	($\sim$0.18)	($\sim$1.52)	($\sim$1.70)		
	Fe(100 K)	0.04 ± 0.01	1.91 ± 0.15	1.96 ± 0.16	XMCD	…
	(corrected)	($\sim$0.09)	($\sim$2.08)	($\sim$2.17)		
Co_3FeN	Co(0 K)	…	1.41	…	Calculation	…
	Fe(0 K)	…	3.09	…	Calculation	…
Co_4N	Co(0 K)	…	1.61	…	Calculation	26
	Co(300 K)	0.08	1.40	1.48	XMCD	22
Fe_4N	Fe(0 K)	…	2.29	…	Calculation	27
	Fe(5 K)	0.17	1.98	2.15	XMCD	20

implies that both Co and Fe atoms are located at both I and II sites in the Co_3FeN film. In order to obtain high spin-polarized Co_3FeN, optimization of the growth conditions is required to prevent the disorder of Co-Fe atoms in the Co_3FeN films.

In summary, the first-principles calculation showed that the $|P|$ value at E_F is decreased when the Co and Fe atoms are located differently from the ideal case. HAXPES and XMCD measurements for the MBE-grown Co_3FeN film were performed and those VB structure and magnetic moments were evaluated. Line shape of the observed photoemission spectrum was well fitted to the calculated spectrum based on the DOSs of Co-Fe replaced Co_3FeN. Magnetic moments per Co and Fe atoms in the Co_3FeN film deduced by sum-rules analysis were close to those in Co_4N and Fe_4N, respectively. These results show that the Co and Fe atoms occupy both the corner and face-centered sites in the Co_3FeN film.

[1]S. Kokado, N. Fujima, K. Harigaya, H. Shimizu, and A. Sakuma, Phys. Rev. B **73**, 172410 (2006).
[2]Y. Imai, Y. Takahashi, and T. Kumagai, J. Magn. Magn. Mater. **322**, 2665 (2010).
[3]K. Ito, K. Harada, K. Toko, H. Akinaga, and T. Suemasu, J. Cryst. Growth **336**, 40 (2011).
[4]Y. Takahashi, Y. Imai, and T. Kumagai, J. Magn. Magn. Mater. **323**, 2941 (2011).
[5]T. Sanai, K. Ito, K. Toko, and T. Suemasu, J. Cryst. Growth **357**, 53 (2012).
[6]H. Xiang, F. Y. Shi, M. S. Rzchowski, P. M. Voyles, and Y. A. Chang, Appl. Phys. A **110**, 487 (2013).
[7]M. C. Payne, M. P. Teter, D. C. Allan, T. A. Arias, and J. D. Joannopoulos, Rev. Mod. Phys. **64**, 1045 (1992).
[8]J. P. Perdew and Y. Wang, Phys. Rev. B **33**, 8800 (1986).
[9]H. J. Monkhorst and J. D. Pack, Phys. Rev. B **13**, 5188 (1976).
[10]D. Vanderbilt, Phys. Rev. B **41**, 7892 (1990).
[11]G. Henkelman, A. Arnaldsson, and H. Jonsson, Comput. Mater. Sci. **36**, 354 (2006).
[12]G. Kresse and D. Joubert, Phys. Rev. B **59**, 1758 (1999).
[13]P. E. Blöchl, Phys. Rev. B **50**, 17953 (1994).
[14]S. Ueda, Y. Katsuya, M. Tanaka, H. Yoshikawa, Y. Yamashita, S. Ishimaru, Y. Matsushita, and K. Kobayashi, AIP Conf. Proc. **1234**, 403 (2010).
[15]R. T. Poole, D. R. Williams, J. D. Riley, J. G. Jenkin, J. Liesegang, and R. C. G. Leckey, Chem. Phys. Lett. **36**, 401 (1975).
[16]K. Ito, K. Okamoto, K. Harada, T. Sanai, K. Toko, S. Ueda, Y. Imai, T. Okuda, K. Miyamoto, A. Kimura, and T. Suemasu, J. Appl. Phys. **112**, 013911 (2012).
[17]Y. Saitoh, Y. Fukuda, Y. Takeda, H. Yamagami, S. Takahashi, Y. Asano, T. Hara, K. Shirasawa, M. Takeuchi, T. Tanaka, and H. Kitamura, J. Synchrotron Radiat. **19**, 388 (2012).
[18]M. B. Trzhaskovskaya, V. I. Nefedov, and V. G. Yarzhemsky, At. Data Nucl. Data Tables **77**, 97 (2001).
[19]Y. Miura, K. Nagao, and M. Shirai, Phys. Rev. B **69**, 144413 (2004).
[20]Y. Takagi, K. Isami, I. Yamamoto, T. Nakagawa, and T. Yokoyama, Phys. Rev. B **81**, 035422 (2010).
[21]K. Ito, G. H. Lee, K. Harada, M. Suzuno, T. Suemasu, Y. Takeda, Y. Saitoh, M. Ye, A. Kimura, and H. Akinaga, Appl. Phys. Lett. **98**, 102507 (2011).
[22]K. Ito, K. Harada, K. Toko, M. Ye, A. Kimura, Y. Takeda, Y. Saitoh, H. Akinaga, and T. Suemasu, Appl. Phys. Lett. **99**, 252501 (2011).
[23]B. T. Thole, P. Carra, F. Sette, and G. van der Laan, Phys. Rev. Lett. **68**, 1943 (1992).
[24]P. Carra, B. T. Thole, M. Altarelli, and X. D. Wang, Phys. Rev. Lett. **70**, 694 (1993).
[25]C. T. Chen, Y. U. Idzerda, H. J. Lin, N. V. Smith, G. Meigs, E. Chaban, G. H. Ho, E. Pellegrin, and F. Sette, Phys. Rev. Lett. **75**, 152 (1995).
[26]S. F. Matar, A. Houari, and M. A. Belkhir, Phys. Rev. B **75**, 245109 (2007).
[27]A. Sakuma, J. Magn. Magn. Mater. **102**, 127 (1991).
[28]R. Nakajima, J. Stöhr, and Y. U. Idzerda, Phys. Rev. B **59**, 6421 (1999).
[29]X. G. Ma, J. J. Jiang, P. Liang, J. Wang, Q. Ma, and Q. K. Zhang, J. Alloys Compd. **480**, 475 (2009).